Electronic Supplementary Material (ESI) for Environmental Science: Nano.


**Supplementary Information**

# Can Mineral Growth by Oriented Attachment Lead to Incorporation of Uranium(VI) into the Structure of Goethite?

Jennifer A. Soltis[a], Martin E. McBriarty[a], Sebastien N. Kerisit[a], Elias Nakouzi[a], James J. De Yoreo[a,] *, and Eugene S. Ilton[a,] *

[a]Pacific Northwest National Laboratory, Richland WA, 99352 USA

*To whom correspondence should be addressed: eugene.ilton@pnnl.gov, james.deyoreo@pnnl.gov

**XRD analysis**

Powder X-ray diffraction patterns measured for each sample were analyzed to estimate the goethite phase fraction in each sample. XRD patterns are shown in **Figure S2**. The appearance of goethite peaks coincident with the largest ferrihydrite peak centered at $2\theta = 16°$ indicates the presence of crystalline goethite, but it seems to be a minority phase. Quantitative analysis of the diffraction patterns, measured in transmission mode, was complicated by (1) the relative difficulty of fitting a ferrihydrite diffraction pattern using standard methods, and (2) a complex background shape due to inconsistent absorption and background shape from the sample holder, an effect most obvious in sample D0-14 as illustrated in **Figure S2**). Thus, the diffraction patterns were analyzed three different ways to estimate the goethite phase fraction. First, XRD patterns for ferrihydrite and goethite standard samples were fitted using existing crystal structure models for goethite[1] and ferrihydrite[2]. Phase fractions were determined by adding these patterns in linear combination with a variable background using either the full $2\theta$ region or only the main peak region ($13.5° < 2\theta < 17.5°$). A third set of fits was performed over $13.5° < 2\ \theta < 19.5°$ using sets of broadened Lorentzian peaks arbitrarily fitted to the diffraction patterns of the ferrihydrite and goethite standard samples. We note that simply refining a goethite pattern with significant peak broadening could not adequately model the sample patterns.

However, the amount of goethite was appreciably less than determined by STEM measurements (see main text). Consequently, we implemented a more rigorous fitting approach to the XRD data by allowing for the size of the goethite particles to shrink in the fit (relative to the goethite standard sample). The result yielded fits with larger goethite phase fractions and are summarized in **Table S1**.

**AIMD-informed EXAFS:**

The EXAFS for the aged samples were analyzed by linear combination fitting (LCF) of a basis consisting of the U-fh standard and simulated EXAFS spectra for U(VI) incorporated in goethite, calculated previously using *ab initio* molecular dynamics (AIMD).[3] Fits were performed using three different simulated spectra for which U(VI) substituted for Fe(III) and charge was compensated by either creating an Fe vacancy at an octahedral site sharing an edge with the U site, removing 3 protons near the U site, or artificially charging the simulated cell. Further details on these simulations and the charge compensation mechanisms can be found in Refs. 3 and 4. The simulated configurations and results of the lcf's are shown in **Tables S2** and **S3**, respectively.

**XANES measurements**

XANES spectra are shown in **Figure S3 (top panel)**. All spectra are qualitatively similar to that of the water-washed uranyl standard sample. However, the water-washed samples are uniformly distinguished from the acid-washed samples by the magnitude of the multiple scattering (MS) shoulder at 17183 eV.[5] No clear relationship (to our knowledge) has yet been established between the magnitude of this feature and the local structure, although a shift in the energy of this MS feature indicates a change in the axial U-O bond lengths,[6] and electrostatic perturbations from the uranyl solvation shell can modify the MS feature.[7] There is no clear connection between the change in the MS feature between the U-fh and acid-washed samples and the EXAFS analysis shown below. However, the MS shoulder is most pronounced for the acid-washed D0 sample set, followed by the acid-washed D7 sample set; these sample sets indeed show subtle differences in the EXAFS (see below).

**Shell-by-shell fitting of the EXAFS data**

As the focus of this work is on the possible incorporation or occlusion of uranium into the iron (oxyhydr)oxide, our EXAFS analysis focuses only on the acid-washed samples; however, we use the water-washed uranyl standard to constrain some features of the EXAFS analysis. The EXAFS data for all acid-washed samples (**Figure S3, bottom panel**) are very similar to the uranyl-sorbed ferrihydrite standard sample, indicating that a majority of U retains the uranyl configuration upon reaction with ferrihydrite under these reaction conditions. The most significant differences are observed in the amplitude minimum and maximum near $k$ = 4.1 and 5.2, respectively. While the amplitudes of all D7 samples closely match the U-fh standard, the amplitudes of the D0 samples are smaller. In previous work on complex, multi-component uranyl systems, such smaller amplitudes (and resultant smaller magnitudes in the EXAFS Fourier transforms $|\chi(R)|$) have indicated configurational disorder due to the presence of multiple similar but distinct coordination environments.[4] This subtle change suggests a physical-chemical difference between the D0 and D7 sample sets.

To determine the cause of the differences, EXAFS spectra were fit using the ARTEMIS program, part of the DEMETER 0.9.26 package.[8] Fits were performed by first simulating an ensemble of photoelectron scattering paths using FEFF, then selectively relaxing or fixing parameters including the scattering path lengths R, path degeneracies (coordination numbers) CN, disorder parameters $\sigma^2$, and the general fit parameters for the overall scattering amplitude $S_0^2$ and binding energy offset $\Delta E_0$. Simultaneous fits to $k^2\chi(k)$ and $k^3\chi(k)$ were performed over the range $4.0 < k < 11.5$ Å$^{-1}$, defined by a Hanning window with 1 Å$^{-1}$ sills.

Because EXAFS analysis of complex systems with multiple bond lengths (such as adsorbed uranyl) is hampered by the statistical limitations of fitting multiple parameters to a single data set,

simplifying assumptions and constraints were applied to the model such that quantitative trends could be identified and linked to the physico-chemical behavior of adsorbed U. A two-stage fitting process was used to minimize correlated parameters. The photoelectron scattering paths and starting assumptions for the initial fit to the uranyl-adsorbed ferrihydrite standard spectrum were as follows:

- One axial oxygen shell (U-$O_{ax}$) represented single scattering from the uranyl bonds, with the CN fixed to 2.[9]
- Three multiple scattering (MS) paths corresponding to the *trans*-dioxo arrangement of the U-$O_{ax}$ bonds were included, each with an effective path length fixed to twice the U-$O_{ax}$ scattering path length. Two of the MS paths, U→$O_1$→U→$O_2$→U (forward scattering through the absorbing U) and U→$O_1$→$O_2$→U (non-forward scattering), had their disorder parameters fixed to 2× $\sigma^2$(U-$O_{ax}$), and the third MS path, U→$O_1$→U→$O_1$→U (rattling), had its disorder parameter fixed to 4× $\sigma^2$(U-$O_{ax}$), as explained in Ref. 5.
- One equatorial oxygen shell (U-$O_{eq}$) was included. In real systems, uranyl species have between four- and six-fold equatorial coordination (between six- and eight-fold total U-O coordination).[9] In real systems, this shell may be split into multiple different bond lengths; this is represented as a large fitted $\sigma^2$(U-$O_{eq}$) parameter.
- A MS path corresponding to U→$O_{ax}$→$O_{eq}$→U was also included. The path length was calculated assuming that the $O_{eq}$ plane is perpendicular to the $O_{ax}$ axis, and the disorder parameter was calculated as $\sigma^2$(U-$O_{eq}$)+$\frac{1}{2}$ $\sigma^2$(U-$O_{ax}$).
- The adsorption of carbonate or other carbonaceous species to uranyl likely occurs during sample preparation, so U-C interactions at around 2.9 Å were included.
- A U-Fe path of about 3.1 Å was also included.

Fits were initially performed to the uranyl-sorbed ferrihydrite standard with all parameters except CN(U-$O_{ax}$), $S_0^2$, and $\sigma^2$(U-C) allowed to relax. $S_0^2$ was fixed to the theoretical value of 0.909 determined previously.[3] $\sigma^2$(U-C) = 0.003 $Å^{-3}$ was chosen based on consensus of prior literature,[10-14] since unconstrained fits resulted in unrealistically large values of $\sigma^2$(U-C) and CN(U-C), which are positively correlated. The fit quality is assessed by an R-factor, but different datasets with different degrees of noise preclude the comparison of fits across data sets. The fitted values from unconstrained "master fits" to the uranyl-sorbed ferrihydrite standard have large uncertainties due to correlations between variables, especially between CN and $\sigma^2$. The fitted values of $\sigma^2$(U-$O_{eq}$) and $\sigma^2$(U-Fe) were therefore fixed for all further fits, along with $\Delta E_0$ (which should be roughly the same for all spectra; see **Fig. S3**) and R(U-C) (to constrain the weakly scattering U-C shell). Results are shown in **Table S4** and **Figure S4**. Comparison of the uncertainties from the master fits and subsequent fits indicate that the final fit model is reasonably well constrained.

The physical significance of the U-Fe and U-C shells may be questioned based on the large uncertainties in their CNs, so additional fits were performed without these shells. Removing the U-Fe shell from the fit (**Table S5** and **Figure S5**) results in a significant drop in CN(U-C). This suggests that the U-Fe and U-C shells encounter some cancellation, such that the sum of the best-fit U-Fe and U-C shells in the all-shell model resembles the best-fit U-C shell in the "noFe" model. However, the fitted parameters in the U-$O_{ax}$ and U-$O_{eq}$ shells are barely affected. In contrast, if the U-C shell is removed, no reasonable parameters for the U-Fe shell can be obtained through fitting. Removing both the U-C and U-Fe shells, and therefore only including the U-O single scattering and multiple scattering paths, yields reasonable fits to the data with little change in the U-O shell parameters (**Table S6** and **Figure S6**).

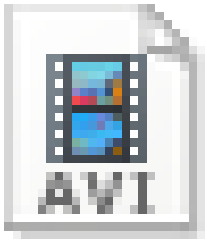


TrackAtoms_U_fh_IND.avi

**Movie 1**: Time-lapsed electron STEM-HAADF images showing diffusion of U atoms under the e beam (see Methods in main text for details). Circles mark the detected particles. Click on icon to start the movie.

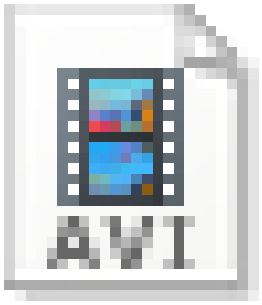


TrackAtoms_U_fh_IND.avi

**Movie 2**: Time-lapsed electron STEM-HAADF images showing diffusion of U atoms under the e beam (see Methods in main text for details). Open circles mark the detected particles and smaller filled circles with the same color show previous particle detections. Click on icon to start the movie.

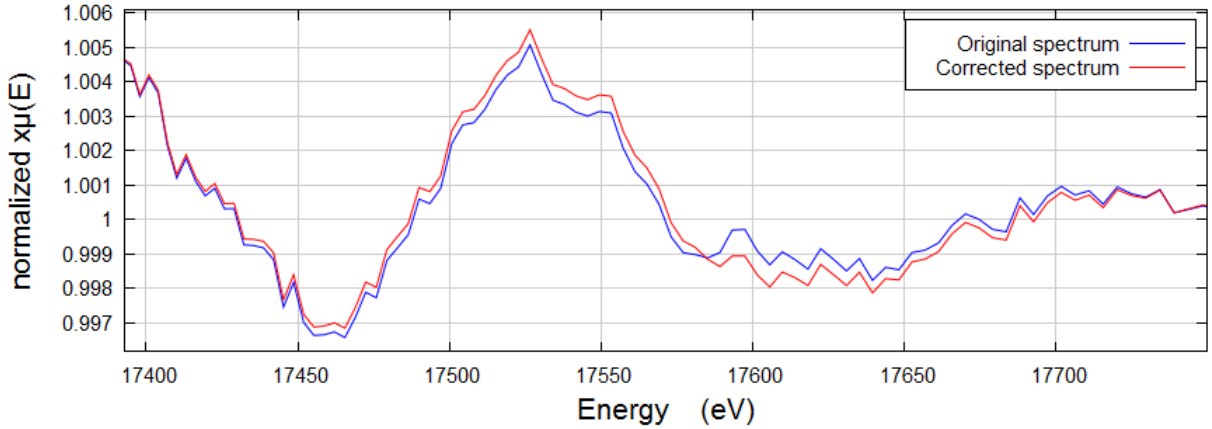


**Figure S1**. Effect of multi-electron excitation correction on the normalized Δ(E) spectra. See methods in main text and Hennig[15].

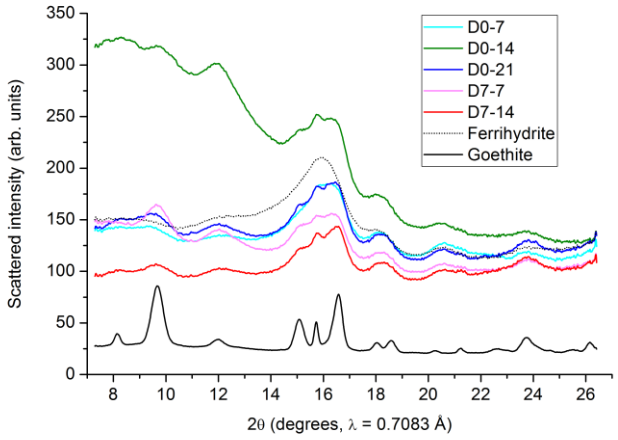


**Figure S2**. XRD patterns for the acid-washed samples as well as two standard samples. The goethite standard pattern has been reduced in scale by a factor of 5.

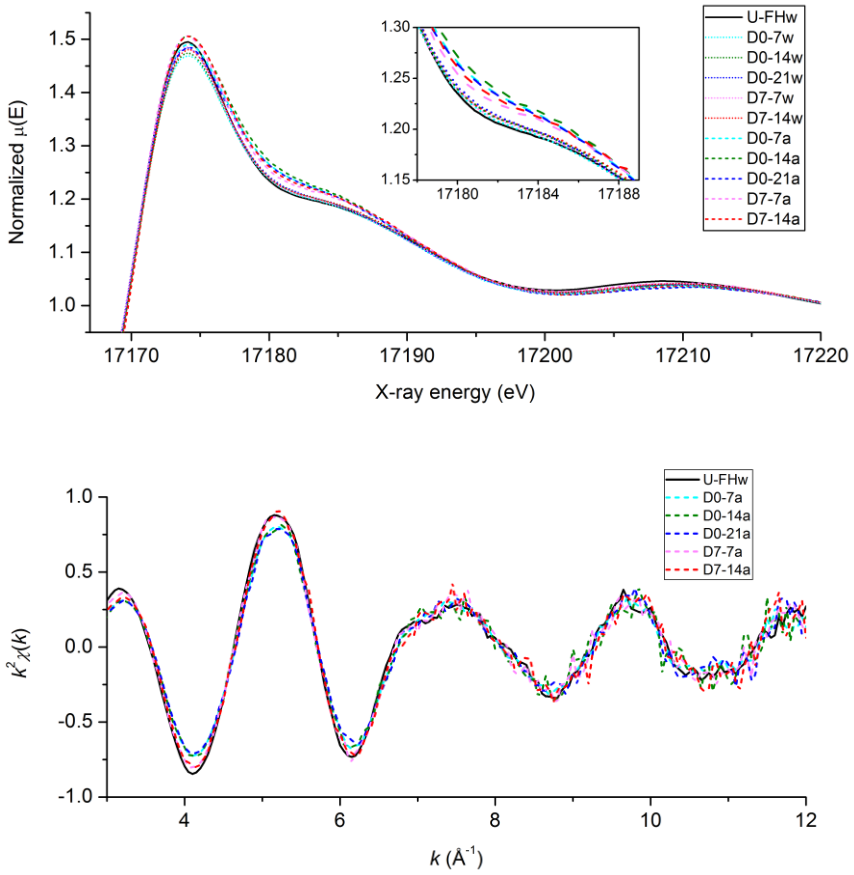


**Figure S3**. XANES (top) and EXAFS (bottom) spectra for all measured samples, including U-ferrihydrite (U-Fh). "w" and "a" indicate "water" and "acid" washes, respectively. See main text for more information.

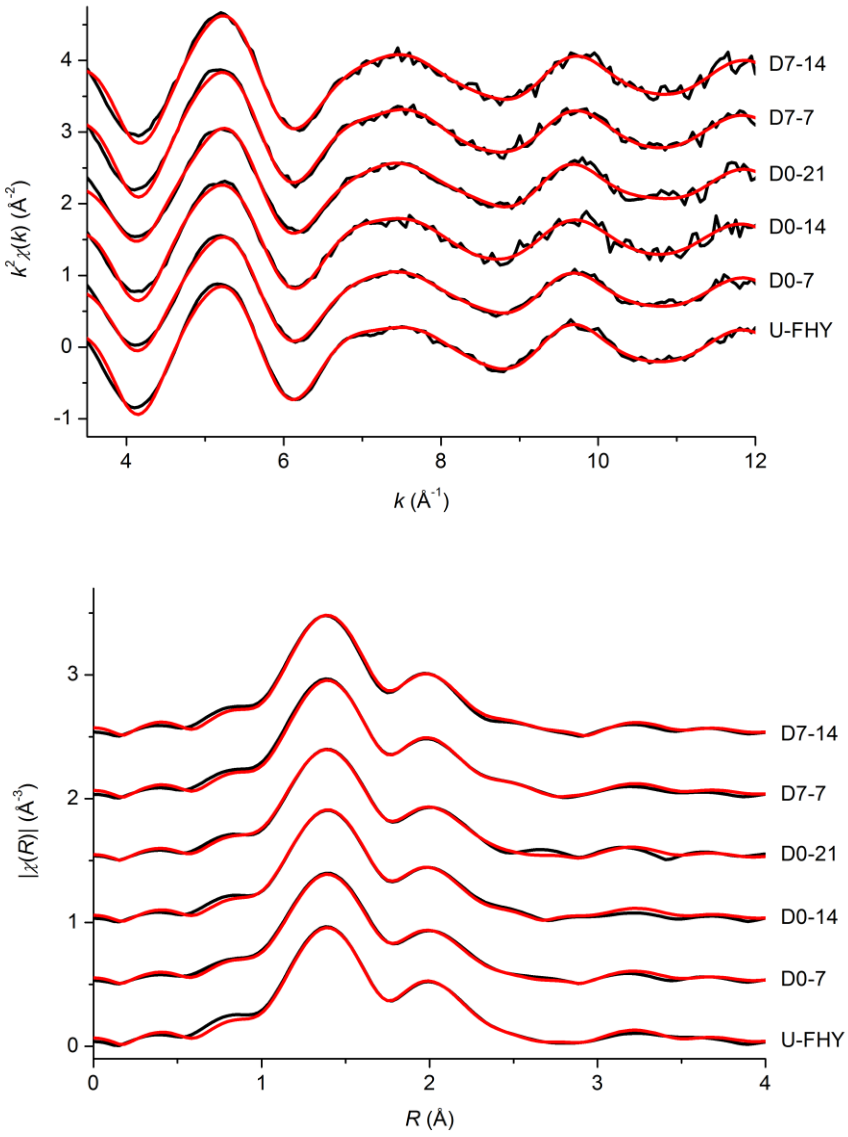


**Figure S4**. Data (black) and fits (red) with parameters from Table S4 for all investigated samples. Original $k^2$-weighted EXAFS spectra (top) are shown along with their Fourier transforms (bottom).

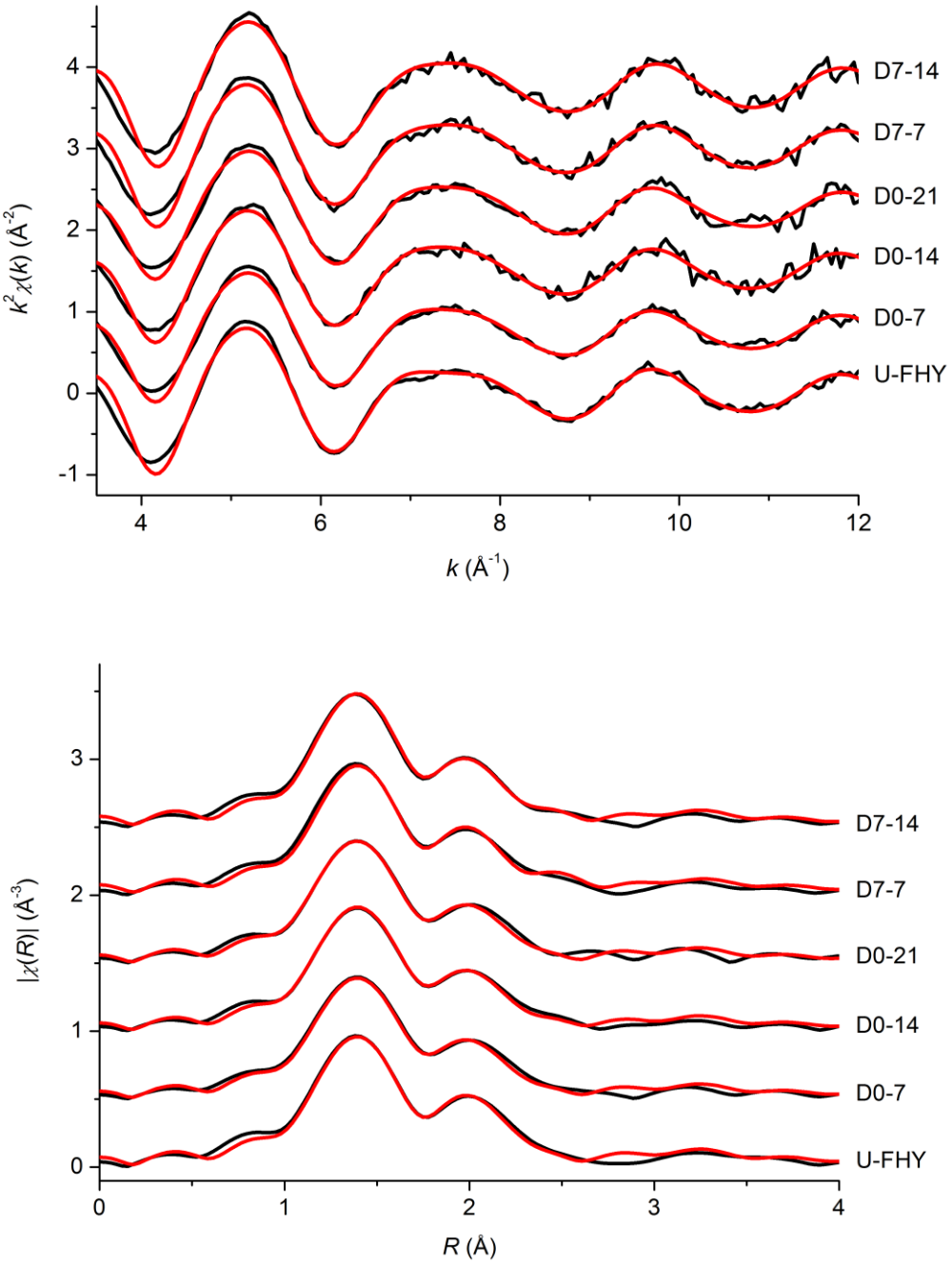


**Figure S5**. Data (black) and fits (red) with parameters from Table S5 for all investigated samples. Original $k^2$-weighted EXAFS spectra (top) are shown along with their Fourier transforms (bottom).

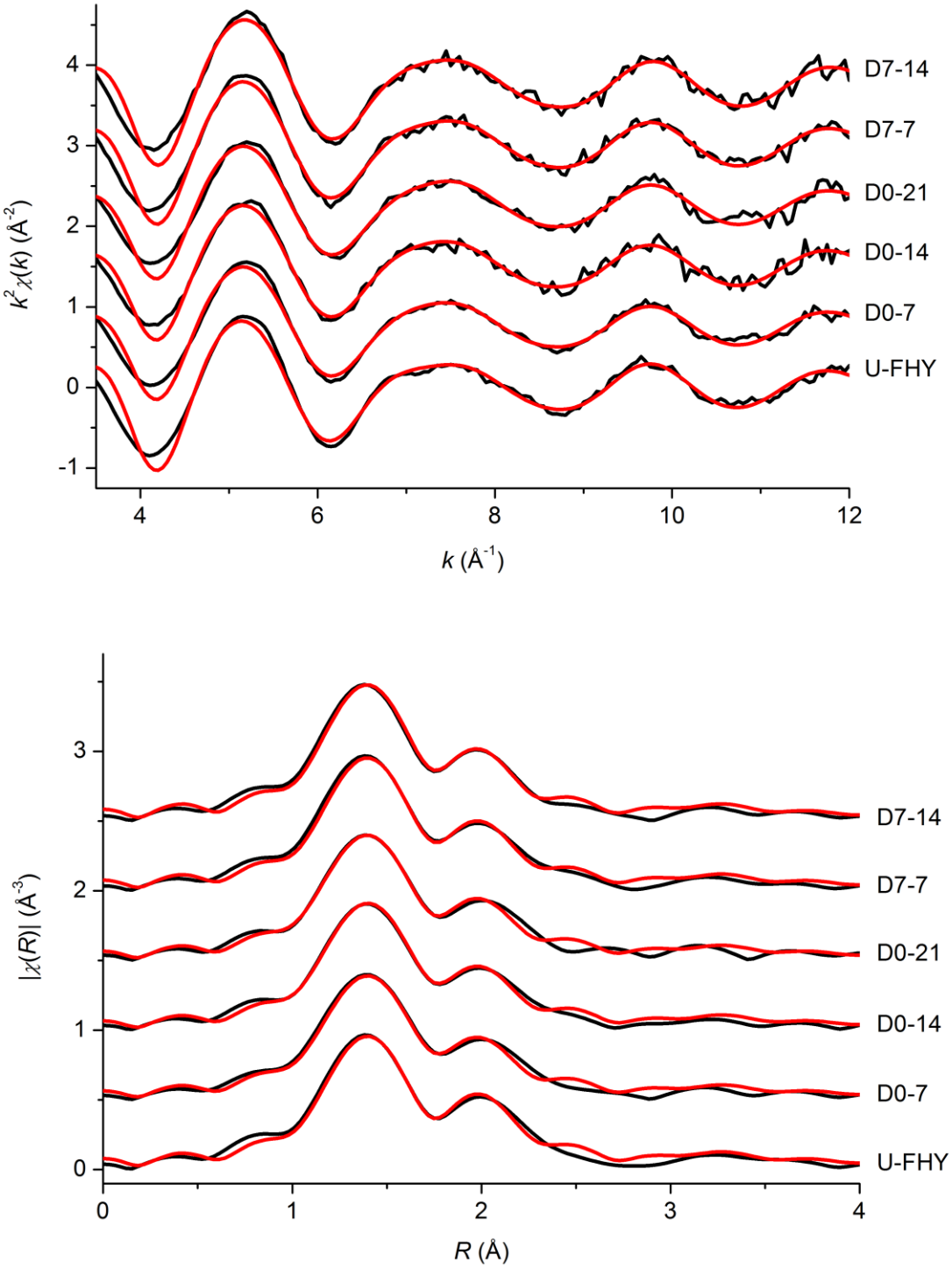


**Figure S6**. Data (black) and fits (red) with parameters from Table S6 for all investigated samples. Original $k^2$-weighted EXAFS spectra (top) are shown along with their Fourier transforms (bottom).

| | Percent phase fraction of goethite | | |
|---|---|---|---|
| Sample | Acid-washed | Water-washed | **Average** |
| D0-7 | 42(4) | 36(6) | **39(5)** |
| D0-14 | 46(23) | 39(1) | **39(1)** [43(14)] |
| D0-21 | 43(2) | 34(4) | **43(2)** [39(6)] |
| D7-7 | 37(1) | 50(5) | **43(8)** |
| D7-14 | 60(3) | 46(7) | **53(9)** |

**Table S1**. Percent phase fraction of goethite in acid-washed and water-washed samples, as well as the average of both acid- and water-washed samples, as measured by X-ray diffraction. Values are presented as averages (with standard deviations in parentheses) of phase fractions determined using three different fitting routines.

| Shell | U−O | | U−$Fe_{eso1}$ | | U−$Fe_{eso2}$ | | U-$Fe_{cso}$ | |
|---|---|---|---|---|---|---|---|---|
| CCS | $\langle r \rangle$ (Å) | $\sigma^2$ (Å$^2$) | $\langle r \rangle$ (Å) | $\sigma^2$ (Å$^2$) | $\langle r \rangle$ (Å) | $\sigma^2$ (Å$^2$) | $\langle r \rangle$ (Å) | $\sigma^2$ (Å$^2$) |
| $V_{Fe}$ | 2.050 | 0.009 | 3.096 | 0.003 | 3.154 | 0.004 | 3.681 | 0.007 |
| −3 $H^+$ | 2.046 | 0.004 | 3.079 | 0.003 | 3.164 | 0.004 | 3.632 | 0.011 |
| UBC | 2.047 | 0.003 | 3.094 | 0.003 | 3.207 | 0.004 | 3.639 | 0.006 |

**Table S2.** Ensemble averages of uranium(VI)–oxygen and uranium(VI)–iron distances and the corresponding disorder parameters for the three CCS considered in this work, as obtained from PBE0 AIMD simulations at 300 K. The terms “eso” and “cso” represent edge-sharing and corner-sharing octahedra, respectively.

| CCS | Sample | $f_{unl}$ | $f_{inc}$ | ΔE (eV) | $\chi^2$ | R-factor |
|---|---|---|---|---|---|---|
| $V_{Fe}$ | D0-7 | 0.943(7) | 0.057(4) | -10 | 0.0014 | 0.0108 |
| | D0-14 | 0.947(8) | 0.053(10) | -10 | 0.0047 | 0.0359 |
| | D0-21 | 0.927(8) | 0.073(6) | -10 | 0.0026 | 0.0204 |
| | D7-7 | 0.988(5) | 0.012(7) | 0 | 0.0023 | 0.0156 |
| | D7-14 | 0.983(7) | 0.017(7) | -10 | 0.0035 | 0.0229 |
| -3 $H^+$ | D0-7 | 0.956(7) | 0.044(4) | -10 | 0.0016 | 0.0126 |
| | D0-14 | 0.959(8) | 0.041(7) | -10 | 0.0049 | 0.0374 |
| | D0-21 | 0.944(8) | 0.056(5) | -10 | 0.0029 | 0.0232 |
| | D7-7 | 0.991(5) | 0.009(5) | -6 | 0.0023 | 0.0158 |
| | D7-14 | 0.985(6) | 0.015(9) | -10 | 0.0034 | 0.0227 |
| UBC | D0-7 | 0.959(6) | 0.041(4) | -10 | 0.0017 | 0.0131 |
| | D0-14 | 0.959(7) | 0.041(7) | -10 | 0.0048 | 0.0367 |
| | D0-21 | 0.947(7) | 0.053(5) | -10 | 0.0031 | 0.0245 |
| | D7-7 | 0.991(5) | 0.009(5) | -10 | 0.0024 | 0.0159 |
| | D7-14 | 0.986(9) | 0.014(6) | -10 | 0.0035 | 0.0228 |
| **Averages** | **D0-7** | **0.953(14)** | **0.047(11)** | | | |
| | **D0-14** | **0.955(15)** | **0.045(15)** | | | |
| | **D0-21** | **0.939(17)** | **0.061(14)** | | | |
| | **D7-7** | **0.990(9)** | **0.010(10)** | | | |
| | **D7-14** | **0.985(13)** | **0.015(13)** | | | |

**Table S3**. Two-component linear combination fit results to the acid washed U $L_3$ EXAFS data for aged uranyl-sorbed ferrihydrite. The phase fractions of the uranyl-sorbed ferrihydrite standard ($f_{unl}$) and AIMD-simulated incorporated U(VI) ($f_{inc}$) are given with the error estimated from least-squares linear combination fitting as performed in the ATHENA program.[8] Three different charge compensation schemes (CCS) are used in the simulations to neutralize the charge of U(VI) substituting for Fe(III): the creation of an iron vacancy ($V_{Fe}$), the removal of 3 protons (-3 $H^+$), or a uniform negative background charge (UBC). An artificial binding energy offset parameter ΔE was also applied for each fit; see previous work for details.[3,4] The phase fractions from all three fits were then averaged for each sample, and errors were propagated as the quadrature sum of the fit errors and the standard deviation of the fitted phase fractions. See main text for more information.

| | $U\text{-}O_{ax}$ | | | $U\text{-}O_{eq}$ | | | U-Fe | | | U-C | | | |
|---|---|---|---|---|---|---|---|---|---|---|---|---|---|
| Sample | CN | R (Å) | $\sigma^2$ (Å$^2$) | CN | R (Å) | $\sigma^2$ (Å$^2$) | CN | R (Å) | $\sigma^2$ (Å$^2$) | CN | R (Å) | $\sigma^2$ (Å$^2$) | R-factor |
| U-fh master fit | 2 | 1.81(1) | 0.0014(6) | 5.1(3.8) | 2.44(3) | 0.012(9) | 1.5(8.1) | 3.12(11) | 0.017(60) | 2.3(1.7) | 2.90(11) | 0.003 | 0.0133 |
| U-fh | 2 | 1.810(3) | 0.0014(4) | 5.1(0.7) | 2.44(1) | 0.012 | 1.5(0.9) | 3.12(4) | 0.017 | 2.3(0.8) | 2.90 | 0.003 | 0.0133 |
| D0-7 | | 1.810(3) | 0.0019(4) | 3.9(0.6) | 2.43(1) | | 1.5(0.8) | 3.13(3) | | 2.2(0.7) | | | 0.0123 |
| D0-14 | | 1.811(7) | 0.0017(8) | 4.0(1.2) | 2.43(3) | | 0.8(1.6) | 3.09(14) | | 1.5(1.5) | | | 0.0449 |
| D0-21 | | 1.809(6) | 0.0017(7) | 3.7(1.0) | 2.43(2) | | 2.1(1.4) | 3.14(4) | | 2.6(1.3) | | | 0.0323 |
| D7-7 | | 1.808(5) | 0.0014(6) | 4.4(0.9) | 2.43(2) | | 1.4(1.2) | 3.11(5) | | 1.5(1.1) | | | 0.0235 |
| D7-14 | | 1.805(5) | 0.0012(6) | 4.6(1.1) | 2.42(2) | | 1.7(1.5) | 3.13(5) | | 1.8(1.3) | | | 0.0310 |

**Table S4.** Results from fits to aged acid washed U-fh,gth samples using a model which includes U-Fe and U-C photoelectron scattering paths. Errors on the last one or two reported digits are given in parentheses; values with no reported errors are fixed. $\Delta E_0$ (8.6 eV), R(U-C), $\sigma^2(U\text{-}O_{eq})$, and $\sigma^2$(U-Fe) were fixed based on the U-fh master fit; $S_0^2$ (0.909) was fixed as described in the text. See main text for more information.

| | $U\text{-}O_{ax}$ | | | $U\text{-}O_{eq}$ | | | U-C | | | |
|---|---|---|---|---|---|---|---|---|---|---|
| Sample | CN | R (Å) | $\sigma^2$ (Å$^2$) | CN | R (Å) | $\sigma^2$ (Å$^2$) | CN | R (Å) | $\sigma^2$ (Å$^2$) | R-factor |
| U-fh master fit | 2 | 1.811(9) | 0.0014(5) | 4.9(2.4) | 2.44(2) | 0.012(6) | 1.6(0.9) | 2.90(4) | 0.003 | 0.0194 |
| U-fh | 2 | 1.811(4) | 0.0014(4) | 4.9(0.7) | 2.44(1) | 0.012 | 1.6(0.7) | 2.90 | 0.003 | 0.0194 |
| D0-7 | | 1.812(4) | 0.0019(4) | 3.7(0.6) | 2.43(1) | | 1.4(0.7) | | | 0.0199 |
| D0-14 | | 1.812(6) | 0.0017(7) | 3.8(1.0) | 2.43(2) | | 1.2(1.1) | | | 0.0472 |
| D0-21 | | 1.810(6) | 0.0017(7) | 3.6(1.0) | 2.43(2) | | 1.5(1.1) | | | 0.0444 |
| D7-7 | | 1.810(5) | 0.0014(5) | 4.3(0.8) | 2.43(2) | | 0.8(0.9) | | | 0.0301 |
| D7-14 | | 1.806(5) | 0.0012(6) | 4.5(1.0) | 2.42(2) | | 0.9(1.1) | | | 0.0394 |

**Table S5**. Results from fits to acid washed aged U-fh,gth samples using a model which includes a U-C photoelectron scattering path. Errors on the last one or two reported digits are given in parentheses; values with no reported errors are fixed. $\Delta E_0$ (9.0 eV), R(U-C), and $\sigma^2(U\text{-}O_{eq})$ were fixed based on the U-fh master fit; $S_0^2$ (0.909) was fixed as described in the text. See main text for more information.

| | $U\text{-}O_{ax}$ | | | $U\text{-}O_{eq}$ | | | |
|---|---|---|---|---|---|---|---|
| Sample | CN | R (Å) | $\sigma^2$ (Å$^2$) | CN | R (Å) | $\sigma^2$ (Å$^2$) | R-factor |
| U-fh | 2 | 1.814(8) | 0.0015(6) | 4.2(1.7) | 2.44(2) | 0.010(5) | 0.0290 |
| U-fh | 2 | 1.814(4) | 0.0015(5) | 4.2(0.6) | 2.44(1) | 0.010 | 0.0290 |
| D0-7 | | 1.814(4) | 0.0020(5) | 3.2(0.6) | 2.43(2) | | 0.0285 |
| D0-14 | | 1.815(6) | 0.0018(7) | 3.3(0.9) | 2.43(2) | | 0.0538 |
| D0-21 | | 1.813(6) | 0.0019(7) | 3.1(0.9) | 2.43(2) | | 0.0535 |
| D7-7 | | 1.812(5) | 0.0014(5) | 3.7(0.7) | 2.43(2) | | 0.0345 |
| D7-14 | | 1.809(5) | 0.0013(6) | 3.8(0.8) | 2.42(2) | | 0.0433 |

**Table S6**. Results from fits to acid washed aged U-fh,gth samples using a model which only includes single and multiple photoelectron scattering paths for the axial and equatorial U-O shells. Errors on the last one or two reported digits are given in parentheses; values with no reported errors are fixed. $\Delta E_0$ (9.8 eV) and $\sigma^2(U\text{-}O_{eq})$ were fixed based on the U-fh master fit; $S_0^2$ (0.909) was fixed as described in the text. See main text for more information.

**References**


1 Yang, H., Lu, R., Downs, R. T. & Costin, G. Goethite, [alpha]-feo(OH), from single-crystal data. *Acta Crystallographica Section E* **62**, i250-i252 (2006).

2 Michel, F. M. *et al.* The structure of ferrihydrite, a nanocrystalline material. *Science* **316**, 1726-1729 (2007).

3 Kerisit, S., Bylaska, E. J., Massey, M. S., McBriarty, M. E. & Ilton, E. S. Ab initio molecular dynamics of uranium incorporated in goethite (α-FeOOH): Interpretation of x-ray absorption spectroscopy of trace polyvalent metals. *Inorg. Chem.* **55**, 11736-11746 (2016).

4 McBriarty, M. E. *et al.* Trace uranium partitioning in a multiphase nano-FeOOH system. *Environ. Sci. Technol.* **51**, 4970-4977 (2017).

5 Hudson, E. A., Allen, P. G., Terminello, L. J., Denecke, M. A. & Reich, T. Polarized x-ray-absorption spectroscopy of the uranyl ion: Comparison of experiment and theory. *Phys. Rev. B* **54**, 156-165 (1996).

6 Zhang, L. *et al.* Extraction of local coordination structure in a low-concentration uranyl system by XANES. *J. Synchrotron Radiat.* **23**, 758-768 (2016).

7 Den Auwer, C. *et al.* Theoretical chemical contribution to the simulation of the liii x-ray absorption edges of uranyl, neptunyl and osmyl hydrates and hydroxides. *New J. Chem.* **28**, 929-939 (2004).

8 Ravel, B. & Newville, M. Athena, artemis, hephaestus: Data analysis for x-ray absorption spectroscopy using ifeffit. *J. Synchrotron Radiat.* **12**, 537-541 (2005).

9 Burns, P. C., Ewing, R. C. & Hawthorne, F. C. The crystal chemistry of hexavalent uranium: Polyhedron geometries, bond-valence parameters, and polymerization of polyhedra. *Can. Mineral.* **35**, 1551-1570 (1997).

10 Allen, P. G. *et al.* Multinuclear nmr, raman, EXAFS, and x-ray diffraction studies of uranyl carbonate complexes in near-neutral aqueous solution. X-ray structure of [c(nh2)3]6[(UO2)3(co3)6].Cntdot.6.5h2o. *Inorg. Chem.* **34**, 4797-4807 (1995).

11 Bargar, J. R., Reitmeyer, R. & Davis, J. A. Spectroscopic confirmation of Uranium(VI)−carbonato adsorption complexes on hematite. *Environ. Sci. Technol.* **33**, 2481-2484 (1999).

12 Redden, G., Bargar, J. & Bencheikh-Latmani, R. Citrate enhanced uranyl adsorption on goethite: An EXAFS analysis. *J. Colloid Interface Sci.* **244**, 211-219 (2001).

13 Bernhard, G. *et al.* in *Radiochimica Acta* Vol. 89 511 (2001).

14 Kelly, S. D. *et al.* X-ray absorption fine structure determination of pH-dependent U-bacterial cell wall interactions. *Geochim. Cosmochim. Acta* **66**, 3855-3871 (2002).

15 Hennig, C. Evidence for double-electron excitations in the $L_3$-edge x-ray absorption spectra of actinides. *Phys. Rev. B* **75**, 035120 (2007).